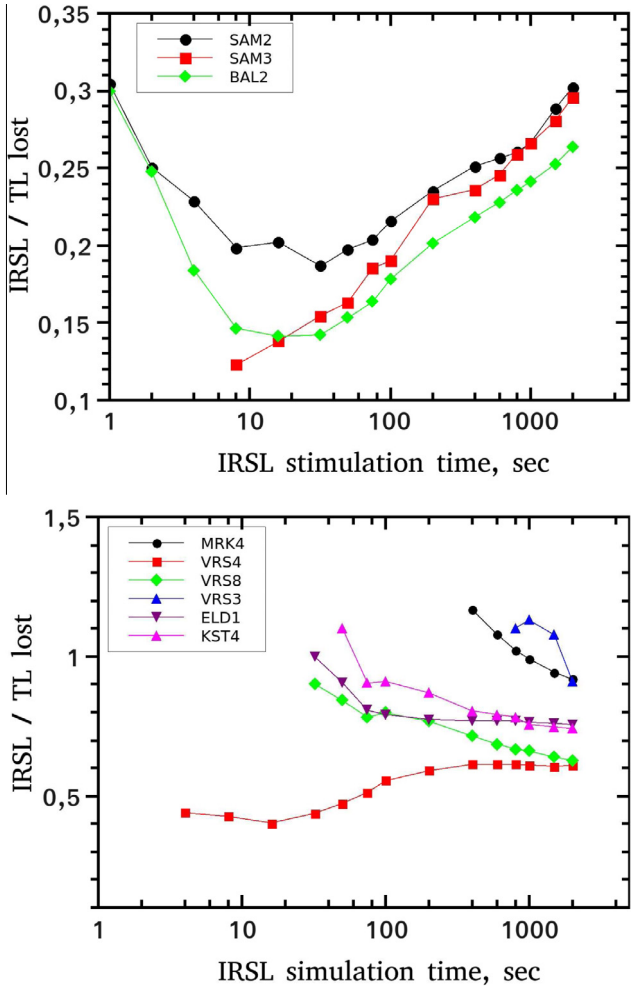

Fig. 6. The ratio of IRSL signal over the difference between the unbleached TL and the R-TL bleached by infrared stimulation, as a function of stimulation time. For the missing points at short stimulation times see Section 3.3.

included in this figure, because this was possible only for a few points at long bleaching times.

The experimental points show a very smooth and continuous behavior, which prompted us to search for an analytical expression to fit them.

The luminescence intensity measured during each one of the stimulation modes can be found as a function of the stimulation time (t_{stim}) as follows. In general the instantaneous luminescence intensity is given by:

$$I(t) = -\frac{dm}{dt}, \tag{1}$$

where $m(t)$ is the concentration of recombination centers. For a localized transition described within the model of Jain et al. [27], one assumes that the concentration of traps $dn/dt \approx dm/dt$, where $n(t)$ is the concentration of carrieres in the ground state. The integrated luminescence signal $I_{integrated}$ for a stimulation time t_{stim} can then be found by integrating Eq. (1):

$$I_{integrated}(t_{stim}) = \int_0^{t_{stim}} I(t)dt = -\int_0^{t_{stim}} \frac{dn}{dt}dt = n(0) - n(t_{stim}), \tag{2}$$

where $n(t_{stim})$ is the concentration of trapped electrons in the ground state at the end of the stimulation process. Kitis and Pagonis [28] showed that within the model of Jain et al. [27], the concentration of electrons during the stimulation process decreases as a function of stimulation time t according to the equation:

$$n(t) = n_0 \cdot exp\left[-\rho'(\ln[1 + zAt])^3\right], \tag{3}$$

with the quantity $A(s^{-1})$ representing the stimulation probability for the infrared or optical stimulation process, and n_o is the concentration of carriers at time $t = 0$. The stimulation probability can also be described as $A = \lambda = 1/\tau$, where τ is the characteristic time constant of each stimulation mode. In this equation ρ' is the dimensionless concentration of charge carriers and $z = 1.8$ is a constant. The stimulation probability is also given by $A = \sigma \cdot I_0$, with σ the IRSL or OSL cross section and I_0 the corresponding stimulation intensity.

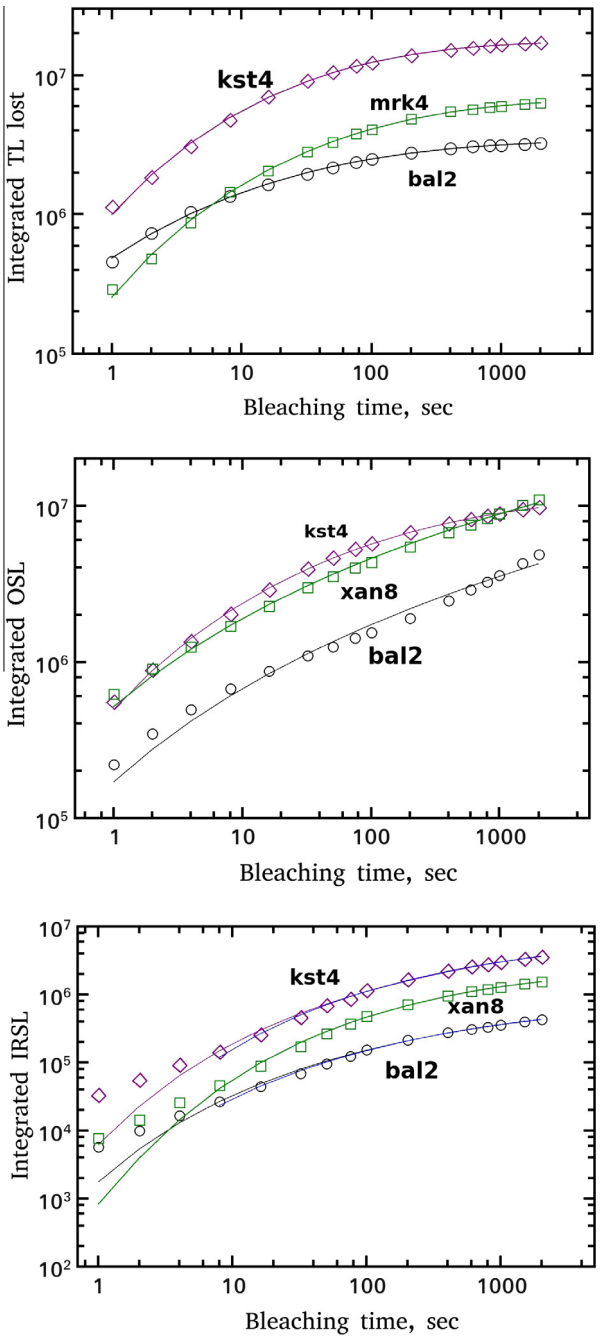

Fig. 7. Growth of the integrated TL lost, OSL and IRSL signals as a function of the bleaching time. The solid lines are the fitting using Eq. (4).

Combining Eqs. (2) and (3):

$$I_{integrated}(t_{stim}) = n_0 \cdot \left(1 - exp\left[-\rho'(\ln[1 + zAt_{stim}])^3\right]\right). \quad (4)$$

Eq. (4) is the analytical expression which was used in the present work to fit the behavior of integrated OSL, IRSL and TL-lost signals as a function of the stimulation time, within the framework of the model by Jain et al. [27].

The results of the fitting are shown by the solid lines through the experimental points in Fig. 7, where one can see the very good fits that are obtained for all signals and for all 10 samples studied. The parameter values obtained from the fitting are listed in Table 2. From the results of Table 2 it is very clear that the sanidine samples sam2, bal2 and sam3 have very different values of A and ρ' than the other two species of K-feldspars studied in this paper. Furthermore, the ρ' values of the OSL for seven of the ten samples are almost an order of magnitude lower than those of the TL-lost and IRSL.

It is not clear what causes this difference between the charge densities. One possible explanation is that the lower values for OSL signals reflect the influence of the band tail states, which one may expect to play a significant role for OSL signals. A second possible explanation is the presence of additional types of hole centers which are accessed in a OSL experiment, but are less accessible during a TL or IRSL experiment. Clearly more work using different samples and different wavelengths is necessary, in order to explain these differences in the density values obtained from TL and OSL experiments.

Moreover, it becomes clear from these Tables that for all three types of luminescence signals the A value shows a decreasing trend, while the ρ' values show in general an increasing trend, with either unit volume or the classification structure parameter $\Sigma T1$. This correlation becomes very obvious especially for the case of the CW-IRSL signals. These results provide a further argument towards the existence of a correlation between the luminescence features and the structural characteristics of K-feldspars.

4.2. Analysis of the decay of R-TL signal with bleaching time

Fig. 8 shows the area under the R-TL glow curves as a function of the bleaching rime.

These curves were also analyzed by fitting them with an analytical expression derived from Eq. (3) as follows. At the end of stimulation process at time t_{stimul}, the number of trapped electrons left in the traps is given by Eq. (3). If one assumes that the TL heating process releases all these electrons and that they recombine with holes, then one would expect the integral of TL glow curves shown in Figs. 1–3 to be proportional to the total number of trapped electrons $n(t_{stimul})$. Therefore the R-TL signals in Fig. 4 should also follow the same Equation i.e.

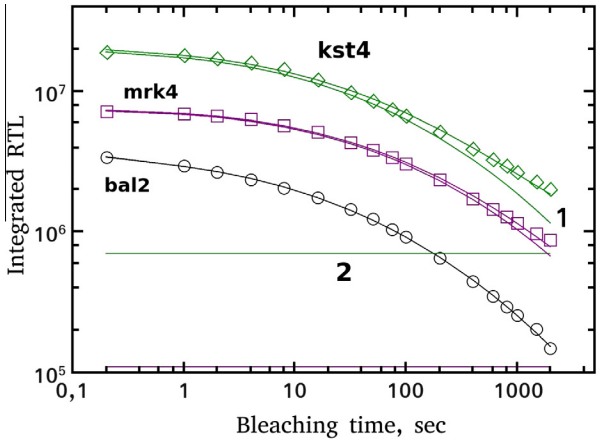

Fig. 8. An analysis example of the R-TL as a function of the OSL bleaching time, using Eq. (5).

$$RTL(t_{stimul.}) = RTL(0) \cdot exp\left[-\rho'(\ln[1 + zAt_{stimul.}])^3\right], \quad (5)$$

where $RTL(0)$ represents the signal at stimulation time $t = 0$. Eq. (5) is used to fit the R-TL decay curves of Fig. 8 using $z = 1.8$ and $A = \lambda = 1/\tau$, where τ is a constant representing lifetime. The constant τ requires some clarification for the present experiments. In the case of CW-OSL or IRSL process the bleaching decay constant $\lambda = 1/\tau$ is equal to $\sigma \cdot I_0$, where σ the photoionization cross-section and I_0 the light intensity. In the case of R-TL although the experimental data concern an integrated TL signal, the R-TL decay curve in Fig. 4 represents the OSL and IRSL bleaching dynamics.

Fitting examples using Eq. (5) along with a stable background are given in Fig. 8. In most case the values of the stable background was negligible as it is seen from the last column of Table 3 which lists the background parameter values resulting from the fitting. In the example of Fig. 8 for sample kst4, the stable background has the second highest contribution of 8%. The highest background contribution observed in this study was for the case of sample vrs3, and was of the order of 20%. On the other hand the lowest contribution of less than 0.1% was observed for samples vrs4 and vrs8.

From the parameter values of Table 3 it is very clear that sanidine samples sam2, bal2 and sam3 have very different values of A and ρ' from the other two species of K-feldspars, in agreement with the results of Table 2 discussed in the previous Section 4.1. Once more, it is not clear what causes this difference between the charge densities. One possible explanation is that the different density values are an artifact of the fitting procedure, since a rather

Table 2
Parameter values of the stimulation parameter $A = 1/\tau$ and ρ' resulted from the fitting of the growth of the integrated signals of TL-lost, OSL, and IRSL as a function of the stimulation time using Eq. (4). The dimension of A is s^{-1}.

	TL lost		OSL		IRSL	
Sample	A	ρ'	A	ρ'	A	ρ'
bal2	43.50	0.0018	27.84	0.00001	0.94	0.0018
sam2	69.80	0.0016	30.29	0.00015	2.11	0.0012
sam3	81.11	0.0015	17.78	0.00013	0.94	0.0018
mrk4	5.43	0.0028	26.96	0.00014	0.63	0.0035
xan8	3.10	0.0034	36.05	0.00012	0.79	0.0024
vrs4	3.44	0.0032	1.61	0.00029	0.17	0.0057
eld1	6.84	0.0042	10.35	0.0011	0.21	0.0066
vrs3	6.01	0.0034	11.35	0.0014	0.31	0.0042
vrs8	3.37	0.0041	8.11	0.00019	0.21	0.0056
kst4	6.78	0.0034	11.36	0.0015	0.48	0.0024

Table 3
Parameters values of the stimulation parameter A and ρ', resulted from the fitting of the R-TL versus OSL bleaching time using Eq. (5). The dimension of A is s^{-1}.

Sample	A	ρ'	Bgr/Eq. (5)
bal2	44.03	0.0018	0.003
sam2	71.88	0.0016	0.05
sam3	81.93	0.0015	0.02
mrk4	10.62	0.0020	0.04
xan8	4.56	0.0027	0.05
vrs4	3.19	0.0034	0.0
eld1	10.11	0.0035	0.048
vrs3	13.46	0.0023	0.2
vrs8	5.09	0.0033	0.0
kst4	20.70	0.0020	0.08

small number of experimental data points is used. A second possible explanation is the presence of several distinct components in the OSL growth and OSL bleaching signals, which would make the accurate determination of the density values less reliable.

4.3. Analysis of CW-OSL and CW-IRSL decay curves

To every bleaching time t_i used in the experimental protocol, corresponds a CW-OSL and a CW-IRSL decay curve. The CW-OSL bleaching can cause either photoionization and then recombination through the conduction band, or excitation to a higher energy level followed again by tunneling recombination. However, the CW-IRSL stimulation can cause only excitation to an excited energy level followed by tunneling recombination. The difference in the efficiency of these processes is clearly shown in Figs. 1–3 especially for long bleaching times.

In this paper we analyze these curves using the localized transition model by Jain et al. [27]. Kitis and Pagonis [28] obtained analytical solutions of the set of differential equations in the model of Jain et al. [27] by using certain mathematical and physical simplifications. These authors presented analytical expressions describing several thermally and optically stimulated luminescence signals within this model. In the case of Continuous wave (CW) simulation the derived analytical expression is:

$$I(t) = \frac{C F(t)^2}{1 + zAt} \cdot exp(-\rho' F(t)^3). \quad (6)$$

$$F(t) = ln(1 + zAt). \quad (7)$$

$$A = \lambda = \frac{1}{\tau}, \quad (8)$$

where C is a constant related to the initial concentration of trapped electrons, and the rest of the symbols have the same meaning as previously defined.

An example of component-resolved CW-OSL decay curve is shown in Fig. 9. As it is seen in Fig. 9 only two tunneling components are needed in order to obtain a high quality fit. The FOM values for the analysis of all samples was less than 1% with a mean around 0.7%. The experimentally measured background was at the level of (45 ± 15) counts/s and has a negligible contribution to the CW-OSL curves. The parameter values resulting from the fitting are listed in Table 4, from which the following conclusions are drawn.

(i) The differentiation in the A and ρ' values of the sanidine feldspar samples observed in Tables 2 and 3 is verified again.
(ii) The ρ' values of the fast component are smaller than the ρ' values of the slow component for the orthoclase and microcline feldspars.
(iii) With the exception of bal2 and sam3 samples, the intensity of the fast component is higher than that of the slow component, as it is seen in the last column of Table 4.

All IRSL decay curves obtained in the present study also consist of two tunneling components, a very fast and intense component, followed by an extended slowly decaying component. In some samples these IRSL decay curves have a peak-shaped form, as shown for selected examples in Fig. 10. This figure shows also the results of the component analysis for typical IRSL decay curves, where one can see that the achieved fittings are excellent. The FOM values for the analysis of all samples were less than 3%. These are higher than the FOM values of CW-OSL signals, due to the lower statistics in the experimental data. The experimentally measured background was about (80 ± 15) counts/s, and is represented by the horizontal line for the bal2 sample, while it is negligible for the eld1 sample.

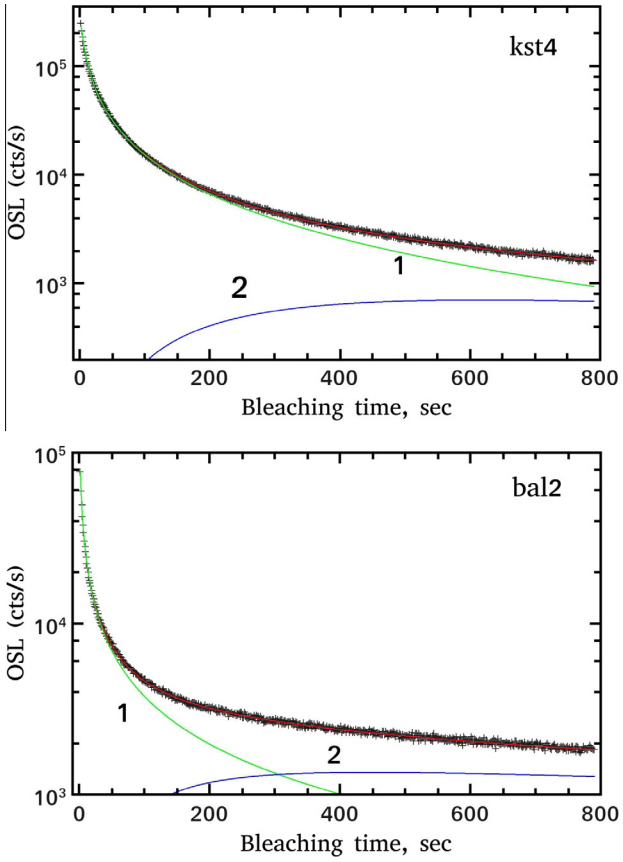

Fig. 9. A component resolved analysis examples of CW-OSL decay curves using Eq. (6).

Table 4
Fitting parameter values of the CW-OSL decay curves using Eq. (6). The dimension of $A = 1/\tau$ is the dimension of τ (s).

Sample	A_1	ρ'_1	A_2	ρ'_2	C_2/C_1
bal2	28.57	0.00065	0.0079	0.00014	0.47
sam2	21.73	0.0006	0.0082	10^{-5}	0.27
sam3	21.73	0.0015	0.015	10^{-5}	0.90
mrk4	31.25	0.00008	0.0074	10^{-5}	0.32
xan8	11.49	0.0007	0.0025	0.099	0.14
vrs4	1.754	0.001	0.0019	0.095	0.26
eld1	1.75	0.0058	0.0028	0.099	0.019
vrs3	2.32	0.0047	0.0027	0.096	0.08
vrs8	2.08	0.0027	0.0002	0.099	0.20
kst4	2.44	0.0041	0.0027	0.078	0.06

The parameter values resulting from the fitting are listed in Table 5. The general conclusions form this table are that.

(i) the differentiation of the sanidine family is not observed in the case of the IRSL signals.
(ii) The ρ' values are at least an order of magnitude higher than those of the OSL signals.
(iii) The ρ' values of the slow components are higher than those of the fast component and
(iv) the relative intensities of the two components listed in the last column of Table 5 vary strongly from sample to sample.

4.4. Behavior of the parameters A and ρ'

The parameter A is related to the stimulation cross section of the luminescence process. In the case of the integrated signals

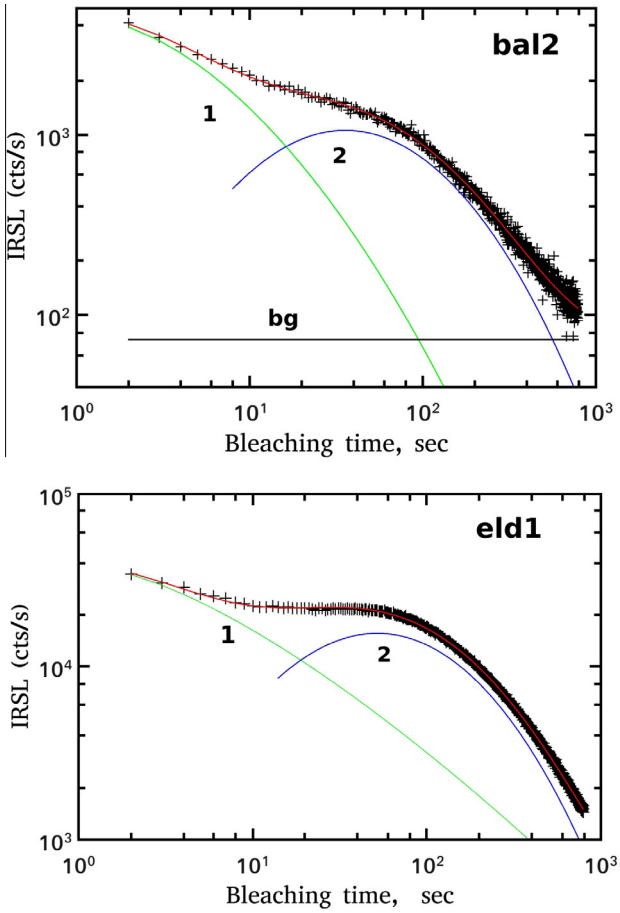

Fig. 10. A component resolved analysis examples of CW-IRSL decay curves using Eq. (6).

(see Tables 2 and 3), the cross section represents a total stimulation cross section for the luminescence signal. In the case of Tables 4 and 5 the parameter A is proportional to the stimulation cross sections from two different energy levels undergoing tunneling recombination. The stimulation cross sections of the fast OSL component for all K-feldspar samples are greater than those of the fast IRSL component, whereas the opposite is true for the slow components. For both components the stimulation cross section of the sanidine feldspars are clearly differentiated from those of the orthoclase and microcline feldspars.

The parameter ρ' is a dimensionless parameter representing the concentration of the luminescence centers. The model of Jain et al. [27] requires that its value must be constant for a given random concentration of donor–acceptor pairs. This is not experimentally verified by the results in this paper, and the ρ' values obtained in the present work show a clear variation for the same K-feldspar sample. Furthermore, the numerical values of ρ' obtained in the present work are in general larger than the values used by Jain et al. [27] for their simulations. The very low numerical ρ' values used by Jain et al. [27] resulted in extremely broad TL glow peaks starting from conventionally low temperatures of 100 °C and ending at extremely high temperatures of 1000 °C. The TL glow-peaks of samples exhibiting anomalous fading (see Figs. 1–3) show normal broad glow peaks, which contain several overlapping TL peaks. Pagonis et al. [44] obtained ρ' values of the order of 0.02–0.03 from fitting of experimental TL glow-curves of feldspars using an analytical expression for TL derived from the model of Jain et al. [27]. Kitis and Pagonis [47] carried out a simulation study of the geometrical properties of TL peaks in the model by Jain et al. [27], and found that the symmetry factor of 0.6 for TL peaks with very low ρ' values drops to a value of 0.5 when ρ' values are increased to a value of about 0.01.

Our results show that different values of ρ' can be expected from analysis of complex TL glow-curves consisting of more than one electron trapping levels. Therefore, more research is needed in order to find the exact information content of the parameter ρ' in the K-feldspars. It is possible that the value of ρ' is related to the magnitude of the anomalous fading effect, which is the most important experimental dosimetric property of feldspars.

Table 5
Fitting parameter values of the CW-IRSL decay curves using Eq. (6). The dimension of $A = 1/\tau$ is the dimension of τ (s).

Sample	A_1	ρ'_1	A_2	ρ'_2	C_2/C_1
bal2	3.22	0.0087	0.064	0.03	0.25
sam2	11.9	0.0004	0.066	0.025	1.4
sam3	4.17	0.0015	0.059	0.037	1.01
mrk4	2.56	0.0230	0.14	0.013	0.09
xan8	2.86	0.0160	0.093	0.016	0.013
vrs4	3.44	0.0000	0.038	0.044	0.37
eld1	4.55	0.0008	0.047	0.035	0.37
vrs3	0.89	0.0840	0.10	0.014	0.03
vrs8	1.28	0.0990	0.12	0.013	0.016
kst4	1.08	0.0001	0.035	0.089	2.52

5. Conclusions – Implications

The conclusions from the present work are summarized as follows:

- The blue light influences simultaneously all electron traps responsible for the TL signal, even from the lowest bleaching time of 1 s. This is due to the ability of blue photons to raise electrons from the traps to either the conduction band by a delocalized transition, or to an excited energy level via a localized transition. Infrared stimulation affects more the low temperature part of the TL glow curve, and its influence decreases gradually as the temperature increases along the TL glow-curve (see Figs. 1, 2 and 4).
- The behavior of the residual TL as a function of OSL or IRSL bleaching time seems to be related to the K-feldspar species each sample belongs to. There is a homogeneous behavior of the sanidine and orthoclase samples, whereas in the case of microclines the behavior of each sample is slightly differentiated, (see Fig. 4).
- Not all electrons escaping from electron traps during OSL and IRSL stimulation contribute to the corresponding OSL or IRSL signal. Therefore, the recombination pathways after thermal, optical and infrared stimulation are different (see Figs. 5 and 6).)
- The growth of the integrated TL-lost, OSL and IRSL signals as a function of bleaching time can be described accurately by the newly developed expressions given by Eq. (4). From the fitting parameters listed in Table 2 it is concluded that the ρ' values are of the order of 10^{-3} for TL-lost and IRSL signals, and of the order of 10^{-4} for OSL. These differences in the ρ' values may be correlated with the anomalous fading rate of these samples.
- The decay of residual TL left after OSL and IRSL stimulation was fitted successfully using Eq. (5).
- The OSL decay curves were fitted using Eq. (6). To the best of our knowledge, this is the first reported fitting of an OSL decay curve in K-feldspars using a localized tunneling recombination model. From the fitting results listed in Table 4, the ρ' values of the fast component for microcline and orthoclase feldspars are smaller than the ρ' values of the slow component.

- The IRSL decay curves were also fitted using the tunneling Eq. (6). From the fitting results listed in Table 5, it is concluded that the ρ' values of the fast IRSL component is smaller than the corresponding ρ' values of the slow component.
- The stimulation cross sections, represented by the parameter A of the fast OSL component for all K-feldspar samples are greater than the A values of the fast IRSL component, whereas the opposite is true for the slow components. For both components the stimulation cross sections of the sanidine feldspars are clearly differentiated from that of the orthoclase and microclines feldspars (see Tables 4 and 5).
- A close relation between the luminescencer properties and the structure of individual feldspar sample in not established clearly. However, the luminescence properties studied in the present work show a very clear differentiation between the three feldspar families.

It is important to note that the experimental data in this paper was analyzed using the model by Jain et al. [27]. However, previous research has shown that band-tail states exist in feldspars and that they play an important role in the production of luminescence signals in these materials. The model used in this paper ignores transitions involving the band-tail states, from which the electrons can recombine with holes via thermal hopping or tunneling. For example, Li and Li [48] studied the thermal stability of the IRSL signal from a sedimentary K-feldspar. They provided an alternative model by considering direct transitions into the band-tail states, and found that their model describes the experimental isothermal data equally well. Also in a recent comparative study of several luminescence models for feldspars, Guralnik et al. [49] discussed several luminescence models for feldspars, and tested these models against isothermal and dose response experimental data. These authors compared the models of Jain et al. [27], of Li and Li [48], as well as a general-order kinetic model, and concluded that all models can provide a reasonable description of the experimental data. Clearly more experimental and modeling work is necessary to obtain a more comprehensive description of luminescence signals in feldspars.

References

[1] A.G. Wintle, Nature 245 (1973) 143.
[2] V. Mejdahl, PACT 9 (1983) 351–364.
[3] V. Mejdahl, Nucl. Tracks Radiat. Meas. 10 (1985) 133–136.
[4] V. Mejdahl, Quaternary Sci. Rev. 7 (1988) 357–360.
[5] A. Zink, R. Visocekas, Radiat. Protect. Dosim. 66 (1996) 399–402.
[6] N.A. Spooner, Quaternary Sci. Rev. 11 (1992) 139–145.
[7] N.A. Spooner, Unpublished D. Phil. thesis, University of Oxford, 1993.
[8] N.A. Spooner, Radiat. Meas. 23 (1994) 625–632.
[9] R. Visocekas, T. Ceva, C. Marti, F. Lafaucheux, M.C. Roberts, Phys. Stat. Sol. (a) 35 (1976) 315.
[10] A.G. Wintle, J. Luminescence 15 (1977) 385.
[11] R. Visocekas, A. Geoffry, Phys. Stat. Sol. (a) 41 (1977) 4993.
[12] R. Visocekas, Nucl. Tracks 10 (1985) 521.
[13] R. Visocekas, Nucl. Tracks Radiat. Meas. 21 (1993) 175–178.
[14] R. Visocekas, N.A. Spooner, A. Zink, P. Blanc, Radiat. Meas. 23 (1994) 371–385.
[15] G. Kitis, P. Bousbouras, C. Antypas, S. Charalambous, Nucl. Tracks Radiat., Meas. 18 (1991) 61.
[16] G.S. Polymeris, N. Tsirliganis, Z. Loukou, G. Kits, Phys. Stat. Sol. (a) 203 (2006) 578.
[17] D.J. Huntley, J. Phys: Condens. Matter 18 (2006) 1359.
[18] G. Hutt, I. Jaek, J. Tchonka, Quaternary Sci. Rev. 7 (1988) 381–385.
[19] P.A. Clark, R.H. Templer, Nucl. Tracks Radiat. Meas. 14 (1988) 139–141.
[20] G.W. Berger, Quaternary Sci. Rev. 7 (1988) 295–303.
[21] N. Tsirliganis, G.S. Polymeris, G. Kitis, V. Pagonis, J. Luminescence 126 (2007) 303.
[22] E. Sahiner, N. Meric, G.S. Polymeris, Radiat. Meas. 68 (2014) 14–22. 2014.
[23] M. Lamothe, M. Auclair, C. Hamzaoui, S. Huot, Radiat. Meas. 37 (2003) 493.
[24] D.J. Huntley, M. Lamothe, Can. J. Earth Sci. 38 (2001).
[25] B. Li, S.H. Li, J. Phys. D: Appl. Phys. 41 (2008), http://dx.doi.org/10.1088/0022-3727/41/ 22/225502 225502.
[26] M. Jain, C. Ankjærgaard. Radiat. Meas. 46 (2011) 292.
[27] M. Jain, B. Guralnik, M.T. Andersen, J. Phys.: Condens. Matter 24 (2012) 385402.
[28] G. Kitis, V. Pagonis, J. Luminescence 137 (2013) 109.
[29] Li, Z. Jacobs, R.G. Roberts, S.H. Li, Geochronometria 41 (2014) 178.
[30] R. Visocekas, Radiat. Prot. Dosim. 100 (2002) 45.
[31] G. Kitis, G.S. Polymeris, V. Pagonis, N.C. Tsirliganis, Radiat. Meas. 49 (2013) 73.
[32] G.S. Polymeris, V. Giannoulatou, I. Sfampa, N.C. Tsirliganis, G. Kitis, J. Luminescence 153 (2014) 245.
[33] G.S. Polymeris, E. Theodosoglou, G. Kitis, N.C. Tsirliganis, A. Koroneos, K.M. Paraskevopoulos, Mediteranian Archaelogy Archaeometry 13 (2013) 155–161.
[34] G.A.T. Duller, A.G. Wintle, Nucl. Tracks Radiat. Meas. 18 (1991) 379–384.
[35] G.A. T Duller, J. Phys. D: Appl. Phys. 28 (1995) 1244–1258.
[36] G.B. Robertson, J.R. Prescott, J.T. Hutton, Nucl. Tracks Radiat. Meas. 21 (1993) 245–251.
[37] R.B. Galloway, Radiat. Meas. 23 (1994) 617–620.
[38] C. Ditlefsen, D.J. Huntley, Radiat. Meas. 23 (1994) 675–682.
[39] G.B. Robertson, J.R. Prescott, J.T. Hutton, Nucl. Tracks Radiat. Meas. 18 (1991) 101–107.
[40] J. Laugier, B. Bochu, Graphical Powder Indexing Cell and Spacegroup Assignment Software, <http://www.inpg.gr/LMGP>.
[41] H. Kroll, P.H. Ribbe, Am. Mineral. 72 (1987) 491.
[42] W.A. Deer, R.A. Howie, J. Zussman, An Introduction to the Rock-Forming Minerals, 2nd ed., Longman, Harlow, 1992.
[43] M.R. Krbetschek, J. Goetze, A. Dietrich, T. Trautmann, Radiat. Meas. 27 (1997) 695–748.
[44] V. Pagonis, P. Morthekai, G. Kitis, Geochronometria 41 (2014) 168.
[45] MINUIT root.cern.ch.
[46] Balian, Eddy, Nucl. Instr. Meth. 145 (1977) 389.
[47] G. Kitis, V. Pagonis, J. Luminescence 153 (2014) 118.
[48] B. Li, S.-H. Li, J. Luminescence 136 (2013) 5.
[49] B. Guralnik, B. Li, M. Jain, R. Chen, R.B. Paris, V. Pagonis, P.G. Valla, F. Herman, Radiat. Meas., In Press. http://dx.doi.org/10.1016/j.radmeas.2015.02.011.